Chapter 6
Modeling of Ultrasound Backscattering by Aggregating Red Blood Cells

Emilie Franceschini and Guy Cloutier

Abstract This chapter provides a review of the last 15 years on the use of quantitative ultrasound (QUS) techniques to characterize red blood cell (RBC) aggregation (i.e., aggregate size, structure and packing organization). The paper focuses on studies aimed at explaining factors affecting the frequency dependent backscatter coefficient (BSC). The theoretical structure factor model of ultrasound backscatter by aggregated RBCs is presented. Computer simulations based on this model are then described to understand the impact of the RBC aggregate size and packing organization on the frequency-dependent BSC. Two QUS cellular imaging methods, based respectively on the structure factor size estimator and the effective medium theory combined with the structure factor model, are compared to estimate the structural aggregate parameters. Finally, in vitro and in vivo results are presented with an optimization method to take into account the attenuation effects of intervening tissues between the probe and the blood flow.

Keywords Cellular imaging · Blood · Red blood cell aggregation · Backscatter coefficient · Structure factor · Effective medium theory · Tissue attenuation

E. Franceschini
Laboratoire de Mécanique et d'Acoustique LMA, CNRS, UPR 7051, Aix-Marseille University, Marseille Cedex 20, Centrale Marseille F-13402, France
e-mail: franceschini@lma.cnrs-mrs.fr

G. Cloutier (✉)
Laboratory of Biorheology and Medical Ultrasonics, University of Montreal Hospital Research Centre (CRCHUM), 2099 Alexandre de Sève (Room Y-1619), Montreal, Quebec H2L 2W5, Canada
e-mail: guy.cloutier@umontreal.ca

G. Cloutier
Department of Radiology, Radio-Oncology and Nuclear Medicine, and Institute of Biomedical Engineering, University of Montreal, Montreal, Quebec, Canada

J. Mamou and M. L. Oelze (eds.), *Quantitative Ultrasound in Soft Tissues*, DOI: 10.1007/978-94-007-6952-6_6,

6.1 Introduction

Blood is a heterogeneous suspension of erythrocytes, leukocytes, and platelets in a fluid plasma. The scattering of ultrasound by blood is mainly attributed to the erythrocytes, also called red blood cells (RBCs), because they constitute the vast majority (97 %) of the cellular content of blood and occupy a large volume fraction (hematocrit) of 35–45 % under normal conditions. RBCs in normal blood flowing through human vessels constitute reversible aggregates. Aggregates usually form rouleaux or complex three-dimensional structures. The mechanisms of aggregate formation and dissociation are complex and depend on the shearing conditions of the flow, the concentration of protein macromolecules in plasma (such as fibrinogen) (Chien 1975; Meiselman 1993; Armstrong et al. 2004) and the RBC aggregability (Rampling et al. 2004). The aggregation phenomenon is normal and occurs in the circulation of many mammalian species. However, hyperaggregation, i.e. an abnormal increase in RBC aggregation, is a pathological state associated with several circulatory diseases such as vascular thrombosis (Chabanel et al. 1994), coronary artery disease (Neumann et al. 1991), diabete mellitus (Poggi et al. 1994; Le Dévéhat et al. 1996), myocardial infarction and cerebrovascular accidents (Hayakawa and Kuzuya 1991; Vayá et al. 2004). The fact that these diseases and their complications generally occur in specific locations of the vascular system suggest a pathological micro- and/or macro-circulatory hemodynamic contribution to their etiologies.

Currently, indices of aggregation can be measured in vitro on samples obtained by venipuncture using different techniques including viscosimetry, erythrocyte sedimentation rate, electrical impedance and light scattering (Stoltz and Donner 1991). Contrary to these techniques needing a withdrawal of blood and the analysis in a laboratory instrument, the ultrasound backscattering method has the potential to measure RBC aggregation under both in vivo and in situ flow conditions. This imaging modality could significantly contribute to the hemorheology field especially at high ultrasound frequencies, since it allows characterization of RBC aggregation in space and in time, as demonstrated by its sensitivity to measure aggregate formation kinetics (Cloutier et al. 2004, 2008) and its ability to follow cyclic aggregation and disaggregation states under pulsatile flows (De Kroon et al. 1991; Nguyen et al. 2008). The ultrasound backscattering method would certainly stimulate prospective clinical studies aimed at elucidating the role of RBC aggregation in the development of cardiovascular diseases and it can also help to improve our basic understanding of the relationship between the hemodynamic of the circulation and RBC aggregation.

Ultrasound and Scatterer Size Estimation

In the ultrasonic blood characterization field, the aim is to obtain quantitative parameters that reflect the RBC aggregation state. One of this relevant quantitative parameter is the aggregate size. It is thus interesting to quickly recall the main quantitative ultrasound (QUS) techniques allowing to estimate scatterer size.

For years, many investigators have attempted to estimate the tissue structure properties (i.e. scatterer size and concentration) by analyzing the power spectra of the radio frequency (RF) data. The access to RF data from laboratory instruments and, increasingly, from clinical scanners allows application of a normalization procedure (Madsen et al. 1984; Wang and Shung 1997) to obtain the backscattering coefficient (BSC), defined as the power backscattered by a unit volume of scatterers per unit incident intensity per unit solid angle. The spectral content of the RF data (and therefore the BSC) contains information about the size, shape, concentration and acoustic impedance of the scattering objects within the tissues. A spectral analysis approach consists in estimating two spectral parameters: the spectral slope and intercept (Lizzi et al. 1986, 1996). The spectral slope is the linear slope of the BSC as a function of frequency on a log-log scale and the spectral intercept is the extrapolation of the BSC linear fit to zero frequency. The slope is related to the effective scatterer size, and the intercept is determined by the scatterer size and acoustic concentration (the acoustic concentration is the product of the scatterer concentration times the square of the relative impedance difference between the scatterers and surrounding tissue). Another QUS method used to extract effective scatterer size and acoustic concentration relies on theoretical scattering models (such as the spherical gaussian model) in order to fit the BSC to an estimated BSC by an appropriate model (Insana et al. 1990). Both spectral analysis and fitting approaches considered random structures, i.e. a low density of scatterers (Lizzi et al. 1986; Insana et al. 1990). These QUS approaches have been successfully used for the characterization of the eye (Feleppa et al. 1986), the prostate (Feleppa et al. 1997), apoptotic cells (Kolios et al. 2002), the breast (Oelze and Zachary 2006) and cancerous lymph nodes (Mamou et al. 2010). However, as will be discussed later (Sect. 6.2), it is not possible to apply these QUS techniques on blood because it is an extremely dense medium (5 million erythrocytes/mm^3) that cannot be considered as random.

Challenges of Ultrasonic Blood Characterization

Besides the high cellular number density of blood, another difficulty for modeling blood backscattering is to consider clustering particles such as RBC aggregates, characterized by specific size, structure and packing organization. Indeed, the structure and packing organization are also relevant QUS parameters for the blood characterization since the structure differs between normal and pathological human RBC aggregates. This was shown by Schmid-Schönbein et al. with microscopic observations of blood samples from normal and diabetic patients (Schmid-Schönbein et al. 1976, 1990) (see Fig. 6.1). The structures of RBC aggregates have the tendency to form clumps (i.e. isotropic structures) in pathological human blood such as in diabetes mellitus, whereas these structures are rouleaux in normal blood (i.e. anisotropic structures).

The aim of the present chapter is to provide a review with an emphasis on the last fifteen years or so on the use of the frequency dependent BSC to characterize RBC aggregation (i.e. aggregate size, structure and packing organization). Before

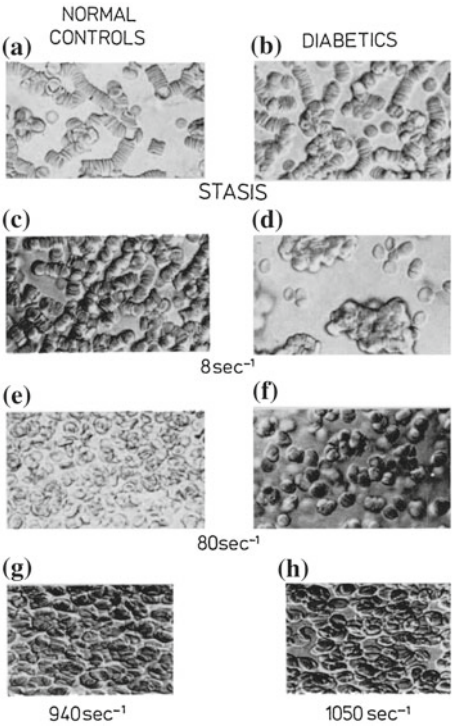

Fig. 6.1 Photomicrographs of normal and pathological RBC aggregation as taken under controlled shear conditions in a transparent rheoscope chamber. At high shear, the cells are dispersed, deformed into ellipsoids, and aligned with their major axes parallel to the direction of the flow (**g**, **h**). As the shear rate is lowered, the aggregates begin to form and assume an equilibrium size which is larger in diabetics than in healthy controls (**e**, **f**). At low shear rate ($8\,s^{-1}$), the normal rouleaux have a stationary size and the hyperaggregating cells in diabetics show a tendency to form clumps (**d**). At stasis, the cells combine into primary rouleaux and into large secondary aggregates (**a**, **b**). Figure reproduced from Schmid-Schönbein et al. (1990)

that, the mean backscattered power or the mean BSC was more generally studied, and the reader can refer to the article of Cloutier and Qin (1997) to have a review on the use of the backscattered power to characterize aggregating RBCs. Section 6.2 presents the structure factor model (Savery and Cloutier 2001; Fontaine et al. 2002) used for modeling aggregated RBCs. In Sect. 6.3, computer simulations of ultrasound backscattering by blood are described based on the structure factor model established in Sect. 6.2. The use of computer simulations allowed to provide information on the impact of the RBC aggregate size and packing organization on the frequency dependent BSC, information that cannot easily be obtained experimentally. In Sect. 6.4, two theoretical backscattering models for the estimation of the structural aggregate parameters are described and their performance are compared based on the computer simulations addressed in Sect. 6.3. Finally, in vitro and in vivo results are presented in Sect. 6.5.

6.2 Backscattering Theory

To model ultrasound backscattering by blood, some simplifying assumptions (but nevertheless acoustically realistic) are necessary. First, it is assumed that shear wave propagation and wave mode conversion are neglected such that only

compressional waves are taken into account. Secondly, attenuation of the backscattered ultrasound blood echoes due to viscous losses is also ignored. As a consequence, the RBCs and plasma are acoustically described as fluid and non-viscous media. Moreover, contrary to the majority of soft tissues, backscattering by blood is also time dependent because of the flow conditions. Nevertheless, one can consider that blood movement is much slower that sound propagation (around 1,540 m/s in blood) such that the insonified blood is quasi-stationary (Mo and Cobbold 1993).

Under the above conditions, two major difficulties for modeling blood backscatter are the high volume concentration of RBCs (i.e. hematocrit) and the clustering of particles. In this section, we indicate how these difficulties have been achieved by presenting successively the ultrasound backscattering from a single RBC, a collection of disaggregated RBCs and aggregated RBCs.

6.2.1 Backscattering Cross Section by a Single RBC Under Rayleigh Condition

Before modeling the ultrasound backscattering by an ensemble of interacting RBCs, it is instructive to model backscattering by a single RBC. A parameter characterizing the ultrasonic signal backscattered by a single scatterer is the differential backscattering cross section per unit volume σ_b, which is the power backscattered by one particle per unit incident intensity per unit solid angle (Mo and Cobbold 1993).

The hemoglobin solution encapsulated by the RBC membrane is acoustically described as a fluid and non-viscous medium, characterized by a compressibility $\kappa_1 = 3.41 \times 10^{-10}\,\mathrm{Pa}^{-1}$ and a density $\rho_1 = 1.092$ g/ml (or equivalently an impedance $z_1 = 1.766$ MRayl and a sound speed $c_1 = 1{,}617$ m/s) (Shung 1982; Savery and Cloutier 2007). The effect of the RBC membrane on acoustical backscattering is neglected because of the small membrane thickness of around 10 nm. The plasma is acoustically described as a fluid and non-viscous medium, characterized by a compressibility $\kappa_2 = 4.09 \times 10^{-10}\,\mathrm{Pa}^{-1}$ and a density $\rho_2 = 1.021$ g/ml (or equivalently an impedance $z_2 = 1.580$ MRayl and a sound speed $c_2 = 1{,}547$ m/s) (Shung 1982; Savery and Cloutier 2007). The RBC is thus considered as a weak scattering medium with a relative contrast of acoustical impedance between the RBC and the plasma equals to $\gamma_z = (z_1 - z_2)/z_2 = 0.13$.

Typical human RBCs are flexible biconcave disks having a diameter of approximately 8 μm and a thickness of 2.2 μm. In most clinical experiments, the ultrasound frequency is in the range of 5–30 MHz, i.e. a wavelength in the range of 50–300 μm. Since the incident wavelength is larger than the size of a RBC, scattering follows the Rayleigh theory. This theory predicts that the backscattering cross-section is proportional to the fourth power of the incident wave frequency and to the square of the scatterer volume, a behavior that does not depend on the

shape of the scatterer (Coussios 2002). Under the Rayleigh scattering theory, the backscattering cross-section σ_b of a single weak scattering RBC is given by (Mo and Cobbold 1993):

$$\sigma_b(-2k) = \frac{k^4 V_s^2}{16\pi^2}\left(\gamma_\kappa - \gamma_\rho\right)^2, \tag{6.1}$$

where k is the wavenumber, V_s the RBC volume, γ_κ the relative contrast in compressibility $\gamma_\kappa = (\kappa_1 - \kappa_2)/\kappa_2$ and γ_ρ the relative contrast in density $\gamma_\rho = (\rho_1 - \rho_2)/\rho_1$. Note that the dependence of σ_b in $(-2k)$ indicates the backscattering configuration where the wave vector is the opposite of the incident wave vector **k**.

In the case of weak scattering, when γ_κ and γ_ρ are very small, the difference between γ_κ and γ_ρ approximates to $\left(\gamma_\kappa - \gamma_\rho\right) \approx -2\gamma_z$. Therefore Eq. 6.1 reduces to:

$$\sigma_b(-2k) = \frac{k^4 V_s^2}{4\pi^2}\gamma_z^2. \tag{6.2}$$

The RBCs are often modeled as scatterers of simple shape such as spheres of equivalent volume. The typical volume of a RBC being 94 μm^3, one RBC can be approximated by a sphere of radius $a = 2.82$ μm. In order to take into account a spherical shape, a spherical form factor F can be added in the expression of σ_b as follows (Insana and Brown 1993; Savery and Cloutier 2007):

$$\sigma_b(-2k) = \frac{k^4 V_s^2 \gamma_z^2}{4\pi^2} F(k) = \frac{k^4 V_s^2 \gamma_z^2}{4\pi^2}\left(3\frac{\sin(2ka) - 2ka\cos(2ka)}{(2ka)^3}\right)^2. \tag{6.3}$$

Savery and Cloutier (2007) compared a semi-analytical model of the backscattering cross section of a realistic biconcave RBC with analytical models of simple shapes (sphere, cylinder, ellipsoid) mimicking a RBC (see Figs. 6.2 and 6.3). This study shows that for frequencies below 21 MHz (i.e. $ka < 0.21$), a RBC can be considered as a sphere of equivalent volume as given in Eq. (6.3). Beyond that limit, the shape and orientation of a RBC could modify the behavior of the backscattering cross-section. However, in practice, when a collection of RBCs randomly oriented is studied, the behavior of the mean backscattering cross section should depend on a mean form factor of the collection of RBCs randomly oriented, such that the limit frequency for the expression of σ_b using the spherical form factor should be above 21 MHz. That is why a collection of non-aggregating RBCs at hematocrits between 6 and 30 % shows experimentally a fourth power frequency-dependence of backscatter up to 30 MHz (Wang and Shung 1997).

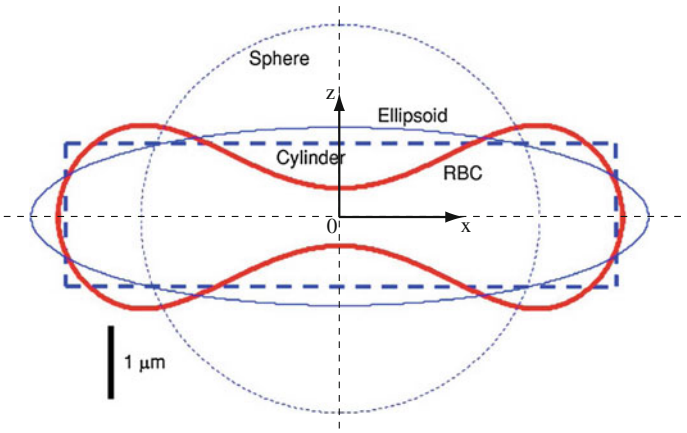

Fig. 6.2 Geometric cross sections of a red blood cell and equivalent descriptive shapes (Figure modified from Savery and Cloutier 2007)

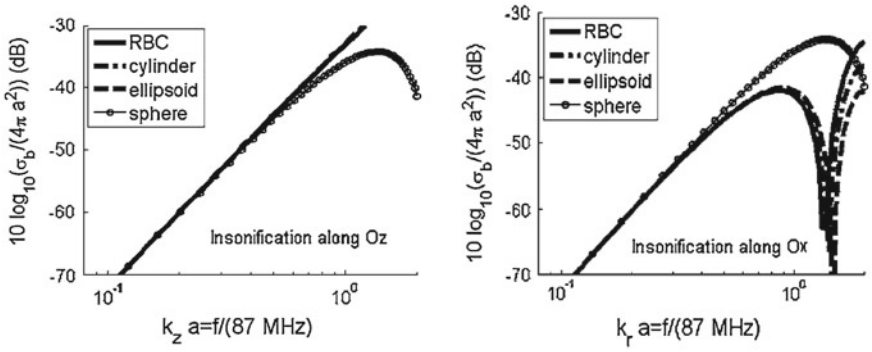

Fig. 6.3 Normalized backscattering cross section with respect to $4\pi a^2$ as a function of the frequency ka for different descriptive shapes and incident wave directions along Oz ($k = k_z$) and Ox ($k = k_r$) (Figure from Savery and Cloutier 2007)

6.2.2 *Backscattering by Disaggregated RBCs: The Particle Model*

The ability of a tissue to generate acoustical echoes is often quantified by the frequency-dependent BSC. In this subsection, we consider a simple case of non-aggregating cells.

For a dilute, random suspension where the volume concentration of particles is typically less than a few percents, each particle equally and individually contributes to the backscattered power. It means that each particle scatters the incident

waves unaffected by the presence of the other particles. The BSC is thus proportional to the average number of scatterers per unit volume n (also called the scatterer density related to the hematocrit ϕ as $n = \phi/V_s$) as follows:

$$BSC(-2k) = n\sigma_b(-2k) \tag{6.4}$$

where σ_b is the backscattering cross section of a single scatterer obtained from Eq. (6.3). However, for human blood at a normal hematocrit (≈ 40 %), even in the absence of aggregation, the RBCs are densely packed. It means that the positions of any pair of scatterers are neither uncorrelated nor perfectly correlated in space and time, such that the RBCs cannot be treated as independent scatterers. In the absence of aggregation, a few stochastic scattering models (Angelsen 1980; Mo and Cobbold 1986, 1992; Twersky 1987; Fontaine et al. 1999), described next, were proposed to better understand the ultrasound backscattered power properties.

Two classical approaches are known as the particle and continuum models. The particle model (PM) consists of summing contributions from individual RBCs and modeling the RBC interaction by an analytical packing factor expression (Mo and Cobbold 1986; Twersky 1987). The continuum model (CM) considers that scattering arises from spatial fluctuations in the density and compressibility of the blood continuum (Angelsen 1980). A hybrid model generalizing the PM and CM frameworks was later proposed by Mo and Cobbold (1992). The RBCs are treated as a single scattering unit within a voxel, which size is defined as a fraction of the acoustic wavelength. The contribution from each single scattering unit is then determined as in the PM, and the contribution from all voxels is then summed by considering the influence of the mean number of scatterers per voxel and its variation in numbers between voxels. A complete description of these models can be found in a review by Mo and Cobbold (1993). Herein we only present in details the PM, which was used as a framework in Fontaine et al. (1999).

The classical approach known as the PM consists of summing contributions from individual RBCs, all considered much smaller than the acoustic wavelength, and modeling the RBC interaction by a packing factor W (Mo and Cobbold 1986; Twersky 1987). Based on this approach, the BSC is given by:

$$BSC_{PM}(-2k) = n\sigma_b(-2k)W. \tag{6.5}$$

The packing factor W can be expressed in terms of the statistical pair-correlation function $g(\mathbf{r})$, which is the probability of finding two particles separated by a distance $\mathbf{r}$:

$$W = 1 + n\int (g(\mathbf{r}) - 1)d\mathbf{r}. \tag{6.6}$$

An example of a pair-correlation function g is shown in Fig. 6.4. The function g is zero at short separations ($r < 2a$), since the particles are impenetrable. Then g oscillates around the value of 1 with several peaks in the range of $r \geq 2a$, with a maximum at $r = 2a$. The occurrence of these peaks at a large range ($r > 2a$)

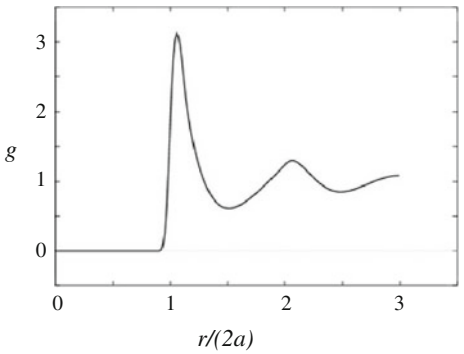

Fig. 6.4 Example of a pair-correlation function g

indicates a high degree of ordering. As the distance r increases, the oscillation of the peaks becomes weak and g tends to a value of 1. Physically, the packing factor W is a measure of orderliness in the spatial arrangement of RBCs. At very low hematocrits, when the RBC positions are completely random, $(g(\mathbf{r}) - 1)$ is equal to 0 and W is equal to unity such that the BSC is simply the sum of the backscattering cross section σ_b from all RBCs. As the hematocrit increases, W decays gradually to zero since closer packing will invariably lead to a greater orderliness in the RBC spatial arrangement. The most often used packing factor expression is based on the Percus-Yevick pair-correlation function for identical, unpenetrable and radially symmetric particles in the m-dimensional (slabs, circles and spheres for $m = 1, 2$ and 3, respectively) (Twersky 1987). The Perkus-Yevick packing factor W_{PY} is dependent on the hematocrit but independent on the frequency. Its value for spheres ($m = 3$) was first applied to blood by Shung (1982) and is given by Twersky (1987):

$$W_{PY} = \frac{(1-\phi)^4}{(1+2\phi)^2}. \tag{6.7}$$

Several studies compared the theoretical BSC_{PM} as a function of the hematocrit with experimental observations (Shung 1982; Lucas and Twersky 1987; Yuan and Shung 1988; Berger et al. 1991). For porcine RBCs suspended in a saline suspension that do not exhibit aggregation (i.e. aggregation does not occur in saline), the PM succeeded to explain the nonlinear relationship between the backscatter amplitude and hematocrit, as shown in Fig. 6.5 (Yuan and Shung 1988). The ultrasonic backscatter versus the hematocrit curve peaks around 13 % as it was expected by the PM using the Perkus-Yevick packing factor given by Eq. 6.7. Comparisons were also conducted on aggregating blood from different species (Yuan and Shung 1988). It is worth noting that the RBC aggregation tendency varies among species (Zijlstra and Mook 1962; Weng et al. 1996a). For example, horse blood has an excessive tendency to aggregate; porcine, dog and normal human bloods have a moderate tendency; and bovine blood forms no aggregate. For bovine whole blood, Yuan and Shung (1988) found that experimental and

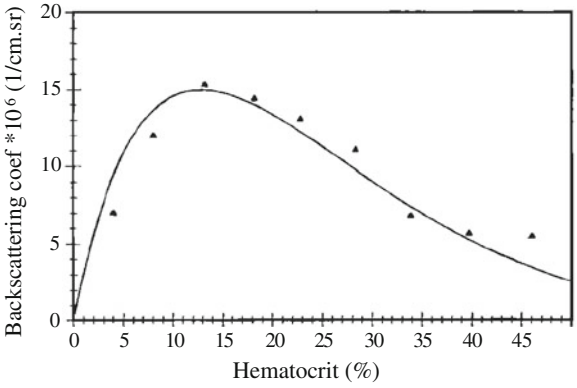

Fig. 6.5 The ultrasonic backscatter from porcine RBC suspensions as a function of the hematocrit. *Solid line* represents theoretical curves calculated from Eq. (6.5) using the Perkus-Yevick packing factor W_{PY}. *Triangles* represent typical experimental results for a laminar flow (Figure modified from Yuan and Shung 1988)

theoretical curves of BSC as a function of hematocrit were qualitatively in good agreement, since the tendency of aggregation is minimal for this blood species. However, to date, no data obtained under RBC aggregation conditions were fitted to the PM.

6.2.3 Backscattering by Aggregated RBCs: The Structure Factor Model

A major difficulty for modeling blood backscattering is to consider clustering particles as RBC aggregates. The aforementioned approach failed to predict the magnitude and frequency dependence of backscatter echoes observed in in vitro experiments when considering aggregating RBCs (Yuan and Shung 1988). Indeed, it was experimentally demonstrated that the aggregated RBCs did not follow a fourth-order frequency dependence contrary to the disaggregated case (Yuan and Shung 1988; Savery and Cloutier 2001). That is why Savery and Cloutier (2001) proposed the Structure Factor Model (SFM) to predict backscattering by aggregating RBCs, by considering first a low hematocrit. This model was later generalized to a normal hematocrit of 40 % (Fontaine et al. 2002). The SFM sums the contributions from individual RBCs and models the RBC interaction by a statistical mechanics structure factor S as follows (Savery and Cloutier 2001; Fontaine et al. 2002):

$$BSC_{SFM}(-2k) = n\sigma_b(-2k)S(-2k) = \frac{\phi}{V_s}\sigma_b(-2k)S(-2k). \tag{6.8}$$

The aggregation phenomenon is only affecting the structure factor S since RBC properties (i.e. σ_b and V_s) and the systemic hematocrit ϕ are expected to remain constant in the modeled region of interest. The structure factor S is by definition linked to the three-dimensional (3D) Fourier transform of the total correlation function $(g(\mathbf{r}) - 1)$:

$$S(-2k) = 1 + n \int (g(\mathbf{r}) - 1) e^{-2j\mathbf{kr}} d\mathbf{r}. \tag{6.9}$$

It can be easily seen by considering the particular case, of an incident plane wave in the x direction of a Cartesian coordinate system (x, y, z) that Eq. (6.9) becomes:

$$S(-2k) = 1 + n \int (g(x, y, z) - 1) e^{-2jkx} dx\, dy\, dz. \tag{6.10}$$

In Eq. (6.10), the structure factor is linked to the standard Fourier transform of the projection, on the ultrasound propagation axis, of the total correlation function. The Fourier transform of the projection is, by the Fourier projection-slice theorem, a line of the 3D Fourier transform of the total correlation function (see appendix of Fontaine et al. 1999). That is why the structure factor S depends only on the modulus k of the wave vector $\mathbf{k}$. Note that the low frequency limit of S is by definition the packing factor W used under Rayleigh conditions. For non-aggregated RBCs under Rayleigh conditions, Eq. (6.8) therefore directly reduces to Eq. (6.5). It is important to emphasize that the structure factor cannot analytically be calculated contrary to the packing factor (Twersky 1987).

The SFM was largely used to perform simulation studies on RBC aggregation as described in the next Sect. 6.3.

6.3 Computer Simulations of Ultrasound Backscattering by Aggregated RBCs

Computer simulation studies have been proposed to better understand mechanisms of ultrasound backscattering by various RBC distributions. First, the backscatter by non-aggregated RBCs as a function of the hematocrit was studied using one-dimensional (1D) and two-dimensional (2D) computer simulations (Routh et al. 1987; Zhang et al. 1994). In these studies, the RBCs are represented by slabs or circles, respectively in 1D or 2D, randomly positioned one by one. Following these studies, Lim and Cobbold (1999) performed 3D computer simulations for non-aggregated RBCs (represented by spheres) and 2D computer simulations for aggregated RBCs. In 3D, the backscattered power of non-aggregated RBCs peaked at around 12 % hematocrit, which corresponds to the PM theoretical prediction and experimental results (Yuan and Shung 1988). In 2D, the mean backscattered power by aggregated RBCs for frequencies below 5 MHz was computed to study the effects of the aggregate size, aggregate compactness and size distribution as a function of the hematocrit. Hunt et al. (1995) performed 1D and 2D computer simulations to study the differences in the backscattered power for several spatial distributions of the scattering sources. These simulations predicted that there would be a large reduction of the backscatter amplitudes if the scattering sources were regularly spaced and that backscatter amplitudes are very sensitive to the degrees of randomness (i.e. random or pseudo-random spatial distribution).

Later, our group performed computer simulations to predict the frequency dependence of the BSC from aggregated RBCs based on the SFM (Teh and Cloutier 2000; Savery and Cloutier 2001, 2005; Fontaine et al. 2002; Fontaine and Cloutier 2003; Saha and Cloutier 2008; Saha et al. 2011; Franceschini et al.2011), contrary to the works previously mentioned which have studied the mean BSC over the studied frequency bandwidth or the integrated backscatter. Our aim was to demonstrate that the use of the BSC frequency dependence would be more powerful than the indices generally used. Most of these simulations were based on particle dynamics or statistical mechanics to obtain the RBC spatial distributions (Savery and Cloutier 2001, 2005; Fontaine et al. 2002; Fontaine and Cloutier 2003; Saha and Cloutier 2008) and had the objective to mimic the rheological behavior of blood. The RBC distributions obtained showed aggregates with various sizes, shapes and compactness. Most of those studies were restricted to two dimensions (Savery and Cloutier 2001, 2005; Fontaine et al. 2002; Fontaine and Cloutier 2003) because of the computational load to generate aggregating RBC distributions. Besides techniques based on particle dynamics or statistical dynamics, another simple and fast method was to randomly generate non-overlapping and identical shaped aggregates (Teh and Cloutier 2000; Saha et al. 2011; Franceschini et al. 2011), as performed previously by Lim and Cobbold (1999). Although this method did not take into consideration realistic interactions between RBCs, it allowed to isolate the effects of hematocrit, aggregate size, shape and/or size distribution on the ultrasound backscattering. In this section, the BSC computation using the SFM is explained and a recent computer simulation that isolates the effects of aggregate size and compactness is presented.

6.3.1 BSC Computation Using the Structure Factor Model

The computation of the BSC_{SFM} using the SFM requires the knowledge of the structure factor S as described in Eq. (6.8). Since the structure factor S is by definition a statistical quantity, an average of all structure factors obtained from several particle distributions can give an estimated value of S.

For each distribution of RBCs, a density matrix M is computed by dividing the square simulation plane L^2 in N_p^2 pixels for a 2D computer simulation (or L^3 in N_p^3 pixels for a 3D simulation) and by counting the number of RBCs falling into each pixel. This matrix represents the microscopic density function defined by

$$M(\mathbf{r}) = \sum_{i=1}^{N} \delta(\mathbf{r} - \mathbf{r}_i) \tag{6.11}$$

where $\mathbf{r_i}$ are the position vectors defining the center of the ith RBC in space, N the number of RBCs in blood and δ the Dirac distribution. An equivalent expression of Eq. (6.9) for the structure factor S can be given in terms of the microscopic density distribution M as follows:

$$S(-2\mathbf{k}) = E\left[\frac{1}{N}\left|\int M(\mathbf{r})e^{-i2\mathbf{k}r}d\mathbf{r}\right|^2\right] \tag{6.12}$$

where E is the ensemble average. The structure factor is thus computed by averaging 2D Fourier transforms for 2D computer simulations (or 3D Fourier transforms for 3D simulations) of several density matrices for averaging purpose. The FFTs give the structure factor values $S(-2\mathbf{k})$ on a centered grid of wave-vectors between $\pm\pi N_p/2L$ with a step of $\Delta k = \pi/L$.

6.3.2 *Effects of the Aggregate Size and Compactness on the BSC Frequency Dependence*

Computer simulations in 2D were recently performed by Franceschini et al. (2011) to isolate, for the first time, the effect of aggregate compactness ϕ_i (i.e. the RBC concentration within aggregates) on the BSC frequency dependence. The simulation algorithm was suitable for generating non-overlapping and isotropic RBC clusters. The locations of the RBCs inside each aggregate were generated randomly to give the desired compactness of aggregates such that the distribution of RBCs within each aggregate was different.

6.3.2.1 Effect of the Aggregate Compactness on the BSC

A key feature of these simulations was the possibility to have various compactnesses of aggregates ϕ_i with the same size of aggregates r_{ag}. Figure 6.6a and b illustrates spatial arrangements of RBCs for a constant value of $r_{ag}/a = 6.32$ (i.e. $r_{ag} = 17.39\,\mu m$), a constant systemic hematocrit $\phi = 20\,\%$ and two compactnesses of aggregates of 40 and 60 %. The corresponding backscattering coefficients BSC_{SFM} were computed with the SFM between 4 and 100 MHz for different aggregate compactnesses of 40, 50 and 60 % at a systemic hematocrit of 20 % (see Fig. 6.6c). As the compactness of aggregates ϕ_i increases, the BSC_{SFM} amplitude increases at low frequencies (< 23 MHz). The first peaks of the BSC_{SFM} are between 18.0 and 20.6 MHz for all simulated conditions.

6.3.2.2 Effect of the Aggregate Size on the BSC

Figure 6.7 shows BSC_{SFM} as a function of frequency for the disaggregated case ($r_{ag}/a = 1$) and for aggregated conditions with radii $r_{ag}/a = 3.16, 5.0$ and 7.07, at different hematocrits. In these simulations, the compactness of aggregates had a constant value of $\phi_i = 60\,\%$. For frequencies less than 20 MHz, the BSC_{SFM}

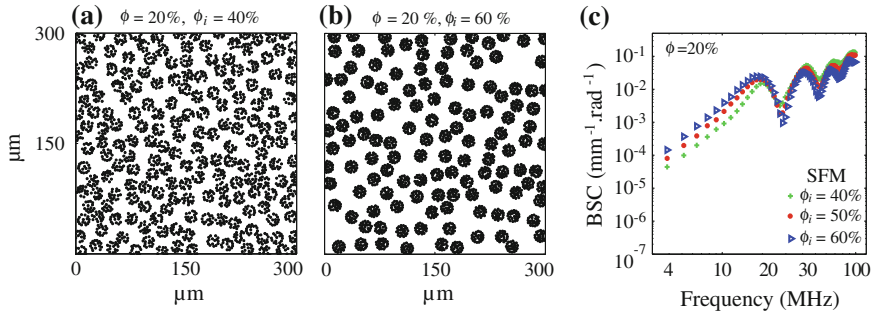

Fig. 6.6 **a** and **b** RBC distributions used in 2D computer simulations for a constant aggregated radius $r_{ag} = 6.32a = 17.32\,\mu m$ and a constant systemic hematocrit $\phi = 20\ \%$ at two aggregate compactnesses: **a** $\phi_i = 40\ \%$ and **b** $\phi_i = 60\ \%$. **c** Dependence of the backscattering coefficients on the compactness of aggregates: $r_{ag}/a = 6.32$ and $\phi = 20\ \%$ (Figure modified from Franceschini et al. 2011)

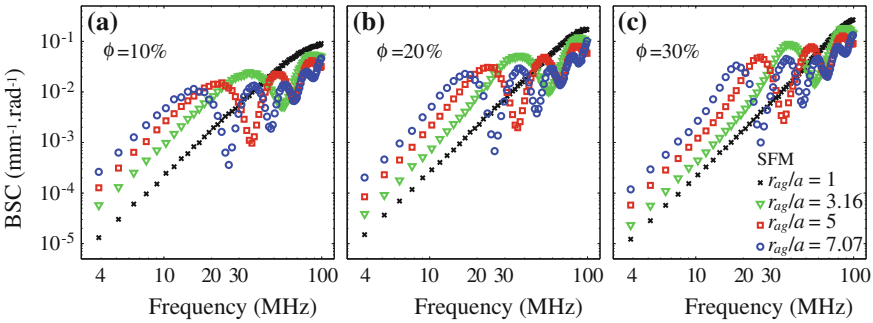

Fig. 6.7 Dependence of the backscattering coefficients for different aggregate sizes and a constant aggregate compactness $\phi_i = 60\ \%$ at systemic hematocrits of 10, 20 and 30 % (Figure modified from Franceschini et al. 2011)

amplitude increases with the size of aggregates. Moreover, the BSC_{SFM} peaks occur at lower frequencies as the aggregate radius increases.

To summarize, this study had provided some insights into the influence of the aggregate size and compactness on the BSC frequency dependence (Franceschini et al. 2011). The aggregate compactness as well as the aggregate size can greatly influence the BSC amplitude. The frequency position of the BSC first peak was found not to be significantly affected by changes in the aggregate compactness, whereas it was greatly affected by changes in the aggregate size. Note that other computer simulations putting emphasis on the influence of the aggregate shape (i.e. anisotropy) and of the aggregate size distribution on ultrasound backscattering can be found in the literature (Lim and Cobbold 1999; Fontaine et al. 2002; Savery and Cloutier 2005).

6.4 Ultrasound Backscattering Modeling for the Estimation of Structural Aggregate Parameters

As seen previously in Sects. 6.2.3 and 6.3, the SFM allows to simulate the BSC from RBCs whatever the RBC spatial distribution (i.e. disaggregated or aggregates with isotropic or anisotropic shape and/or with various aggregate sizes, shapes and compactnesses). However, the SFM can hardly be implemented to estimate structural parameters in the framework of an inverse problem formulation because of the intensive computational time to assess the structure factor by realizing distributions of RBCs with simulations. That is why two scattering theories, named the Structure Factor Size Estimator (SFSE) and the Effective Medium Theory combined with the Structure Factor Model (EMTSFM), have been recently developed in order to approximate the SFM for practical assessments of RBC structural features (i.e., in an inverse problem formulation). Both theories are based on some simplifying assumptions regarding the RBC spatial distributions:

- First, isotropic aggregates are assumed. In human blood, low shear rates can promote the formation of RBC aggregates having anisotropic (i.e. rouleaux) or isotropic (i.e. clump) structures, as seen in Fig. 6.1. The rouleaux like pattern is typically associated to normal blood. However, as the binding energy between RBCs increases with inflammation (Weng et al. 1996b), aggregates form clump structures such as in diabetes mellitus (Schmid-Schönbein et al. 1976, 1990). The assumption of isotropic aggregates is thus valid as far as we are concerned with the study of pathological states.
- Second, a minimal polydispersity in terms of aggregate sizes is assumed. Under in vivo conditions with ultrasound measurements on a blood vessel, the shear rate distribution varies with the radial position, and consequently, the aggregate size distribution too. That is why the backscattered echoes from blood are generally analyzed over a rectangular or a hamming window which is moved along the RF signal to examine the whole vessel at different depths (Yu and Cloutier 2007; Yu et al. 2009). For example, at a central frequency of 25 MHz, the window length was typically around 400 μm (Yu et al. 2009). RBC aggregates may thus be assumed to be locally identical, but variations can be considered within an ultrasound image by moving the measurement window.

6.4.1 Structure Factor Size Estimator

Yu and Cloutier (2007) and Yu et al. (2009) developed the SFSE scattering theory, which consists of using a second-order Taylor expansion of the structure factor as follows:

$$\begin{aligned} S(-2k) &\approx C_0 - 2kC_1 + (-2k)^2 C_2 \\ &\approx W - 4R_g^2 k^2 \\ &\approx W - \frac{12}{5}(kaD)^2 \end{aligned} \tag{6.13}$$

where C_0, C_1, and C_2 are simply the series coefficients. We have shown earlier that C_0 is the low frequency limit of the structure factor, named the packing factor W (see Eq. 6.6), here for aggregated RBCs. By considering isotropic aggregates, the second constant C_1 is equal to zero because the blood remains the same if the blood sample is turned around 180° (i.e. $S(-2k) = S(2k)$). By a dimensional analysis, the third constant C_2 is a surface in m^2 and is assumed to be the square of the mean aggregate gyration radius R_g^2, as usually performed in the field of crystallography using x-ray scattering (Guinier and Fournet 1955; Yu and Cloutier 2007). The diameter of an homogeneous spherical object in terms of number of RBCs can also be related to its radius of gyration as $D = \sqrt{5/3}R_g/a$ (Guinier and Fournet 1955; Yu and Cloutier 2007).

To summarize, the SFSE parameterizes the BSC by two structure indices, the packing factor W and the mean aggregate diameter D assumed to be isotropic, as follows:

$$\begin{aligned} BSC_{SFSE}(-2k) &= n\sigma_b(-2k)\left(W - \frac{12}{5}(kaD)^2\right) \\ &= \frac{\phi}{V_s}\frac{k^4 V_s^2 \gamma_z^2}{4\pi^2}\left(3\frac{\sin(2ka) - 2ka\cos(2ka)}{(2ka)^3}\right)^2\left(W - \frac{12}{5}(kaD)^2\right). \end{aligned} \tag{6.14}$$

Assuming that the hematocrit ϕ, the RBC radius of the equivalent sphere a and the impedance contrast γ_z are known *a priori*, the parameters W and D are estimated by fitting the measured BSC versus frequency with the theoretical BSC_{SFSE} given in Eq. (6.14).

6.4.2 *Effective Medium Theory Combined with the Structure Factor Model*

A new scattering theory, named an Effective Medium Theory (EMT) combined with the SFM (EMTSFM), was recently proposed by Franceschini et al. (2011). The EMT was initially developed by Kuster and Toksoz (1974) in the field of geophysics. Herein, the EMT assumes that aggregates of RBCs can be treated as individual homogeneous scatterers, which have effective properties determined by the concentration of RBCs within aggregates (i.e. the compactness of aggregates ϕ_i) and acoustical properties of blood constituents. The approximation of RBC

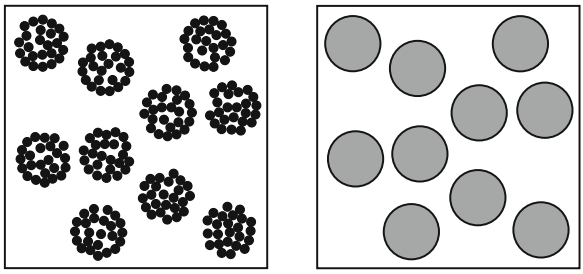

Fig. 6.8 Schematic representation of aggregates treated as individual scatterers. The aggregates of RBCs in blood (*left side*) are assumed to be homogeneous particles (*right side*) with effective properties that depend on the internal hematocrit, and density and compressibility of the RBCs within them (Figure from Franceschini et al. 2011)

aggregates as homogeneous effective particles is combined with the SFM to consider the concentrated blood medium. The effective particle interactions were thus modeled by a structure factor, as in Savery and Cloutier (2001) and Fontaine et al. (2002). The EMTSFM parameterizes the BSC by three indices: the aggregate radius, the concentration of RBCs within aggregates (also named aggregate compactness) and the systemic hematocrit. In the field of clinical hemorheology, assessing the compactness of RBC aggregates is of high clinical importance since it is related to the binding energy between cells. Normal RBC aggregates form rouleaux type structures, whereas pathologies associated with stronger binding energies result in clumps of RBCs (close to a spherical isotropic packing). A complete description of the EMTSFM is described below.

As a first approximation, we assume that all the RBCs are aggregated in blood, that the aggregates are identical and isotropic and that the RBCs within the aggregates are evenly distributed. The EMTSFM assumes that aggregates of RBCs can be treated as individual homogeneous scatterers as shown in Fig. 6.8. Each aggregate is thus approximated by an effective single particle. The density ρ_{ag} and compressibility κ_{ag} of the new effective particle are determined by considering the EMT (Kuster and Toksoz 1974). It means that ρ_{ag} and κ_{ag} are derived from the acoustical properties of the two fluids that constitute the aggregates (i.e. ρ_1, ρ_2, κ_1 and κ_2, where 1 indicates properties of RBCs and 2 those of plasma) and from the internal concentration of RBCs within the aggregates ϕ_i, as follows:

$$\begin{aligned} \rho_{ag} &= \phi_i \rho_1 + (1 - \phi_i)\rho_2 \\ \frac{1}{\kappa_{ag}} &= \frac{\phi_i}{\kappa_1} + \frac{1 - \phi_i}{\kappa_2} \end{aligned} \tag{6.15}$$

The BSC from blood is then obtained by summing contributions from individual effective particles of radius r_{ag} and modeling the effective particle interaction by a

statistical mechanics structure factor S_{ag}. The equivalent BSC expression is thus given by:

$$BSC_{EMTSFM}(-2k) = n_{ag}\sigma_{ag}(-2k)S_{ag}(-2k), \tag{6.16}$$

where n_{ag} is the number density of aggregates that is related to the effective volume fraction of aggregates ϕ_{ag}. The effective volume fraction of aggregates is equal to the volume fraction of RBCs in blood ϕ divided by the aggregate compactness ϕ_i: $\phi_{ag} = \phi/\phi_i$. The backscattering cross-section σ_{ag} of an effective single sphere can be determined using the fluid-filled sphere model developed by Anderson (1950). That model provides an exact solution for the backscattering of sound by a single fluid sphere, not necessarily small compared to the wavelength, in a surrounding fluid medium (i.e. the plasma). The structure factor S_{ag} corresponds here to a collection of N_{ag} identical and disaggregated particles (mimicking RBC aggregates) of radius r_{ag} randomly distributed.

By assuming that the RBC radius a and the acoustical properties of plasma and RBCs are known *a priori*, the unknown parameters are the aggregate radius r_{ag} and aggregate compactness ϕ_i. The unknown parameters can be estimated by matching the measured BSC with the theoretical BSC_{EMTSFM} given by Eq. (6.16).

6.4.3 Assessment of the Accuracy of Scattering Models in Determining the RBC Aggregate Size and Aggregate Compactness

To our knowledge, there is no means to experimentally assess aggregate sizes at 40 % hematocrit because RBCs at that hematocrit are opaque to light. The experimental assessment of accuracy of the SFSE was only performed at a low hematocrit of 6 % by comparing optical and acoustic measurements of RBC aggregate sizes (Yu and Cloutier 2007). That is why 3D computer simulations producing BSCs from RBC aggregates were recently performed to evaluate the accuracy of the SFSE method (Saha et al. 2011). In this subsection, we determine the performance of the EMTSFM to extract RBC aggregate sizes and compactnesses from simulated BSC_{SFM} and compare that with SFSE predictions. This comparison is based on 2D computer simulations using the SFM previously presented in Sect. 6.3. In the following, all the estimated parameters are denoted by a star.

The SFSE and EMTSFM are first examined when the aggregate size is fixed $r_{ag}/a = 6.32$ and aggregate compactnesses ϕ_i vary from 40 to 60 %. Figure 6.9a presents the BSC fitted curves with the SFSE and the EMTSFM to the simulated BSC_{SFM} already presented in Fig. 6.6. The fitted curves using the SFSE overestimate the BSC_{SFM} amplitude at low frequencies, whereas the EMTSFM provides good fittings to the simulated BSC_{SFM}. The values of the estimated parameters W^*

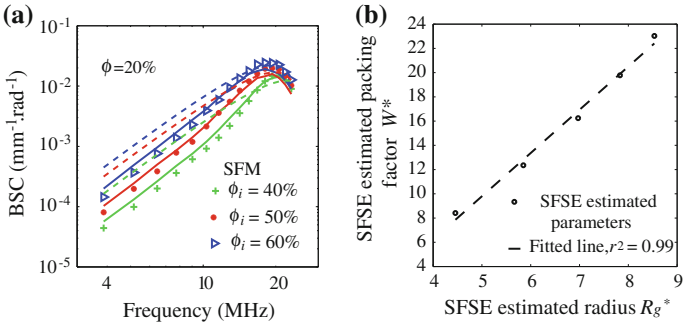

Fig. 6.9 **a** Frequency-dependent backscatter coefficients computed with the SFM for different aggregate compactnesses and a constant aggregate size $r_{ag}/a = 6.32$ at a systemic hematocrit of 20 %, and corresponding fitting with the SFSE (in *dashed lines*) and with the EMTSFM (in *solid lines*). **b** Linear relationship between estimated parameters W^* and R_g^* obtained with the SFSE

and R_g^* obtained with the SFSE and estimated parameters r_{ag}^*/a and ϕ_i^* obtained with the EMTSFM are reported in Table 6.1 for a systemic hematocrit of 20 %. Although the true radius is fixed, the estimated R_g^* increases with the aggregate compactness. A linear relation links also the estimated parameters W^* and R_g^* when the aggregate compactness varies (see Fig. 6.9b), as it was previously observed in Yu and Cloutier (2007) and Saha et al. (2011). Therefore there is no significant correlation between the actual fixed radius and the estimated radii. The SFSE cannot take into account a variation in aggregate compactnesses since a change in compacity is interpreted as a change in the aggregate size. On the other hand, the EMTSFM gives quantitatively satisfactory estimates with relative errors inferior to 8 % for the estimated aggregate size and inferior to 19 % for the estimated compactness.

The SFSE and EMTSFM are also evaluated when the aggregate size varies and the aggregate compactness is fixed to a high value: $\phi_i = 60$ %. Figure 6.10a presents the BSC fitted curves with the SFSE and the EMTSFM to the simulated BSC_{SFM} at a hematocrit of 30 %. The EMTSFM fits very well the simulated BSC_{SFM}, whereas the fitted SFSE curves over-estimate the simulated BSC_{SFM} in the low frequency range. For the SFSE, significant correlations between the estimated and true radii of aggregates with a correlation coefficient r^2 around 0.95 were found for all hematocrits (Fig. 6.10b). The EMTSFM gives quantitatively satisfactory estimates with relative errors inferior to 7 and 14 %, respectively, for the aggregate size and the aggregate compactness, whereas the relative errors for the estimated radii with the SFSE model are comprised between 24 and 62 % (see Table 6.2).

To conclude, although the SFSE did not provide good fits to the simulated data, significant correlations between the estimated and true radii of aggregates with r^2 around 0.95 were found when the aggregate compactness was fixed. However, the SFSE showed no significant correlation between the actual fixed radius and those

Table 6.1 Comparison of the SFSE and EMTSFM based on simulated BSCs for the following aggregating conditions: $r_{ag}/a = 6.32$, $\phi = 20\ \%$, ϕ_i varies

SFM		SFSE			EMTSFM			
Actual r_{ag}/a	Actual ϕ_i (%)	Estimated W^*	Estimated R_g^*	$\varepsilon_{R_g^*}$%	Estimated ϕ_i^* (%)	$\varepsilon_{\phi_i^*}$ (%)	Estimated r_{ag}^*/a	$\varepsilon_{r_{ag}^*}$ (%)
6.32	40	6.49	3.92	37.86	44.56	11.40	5.8	8.23
6.32	50	12.51	6.12	3.01	59.5	19.00	5.9	6.65
6.32	60	17.74	7.49	18.60	67.71	12.85	5.8	8.23

Values of the aggregate size r_{ag}/a and compactness ϕ_i used for computation of the simulated BSC_{SFM} from the SFM, and values of parameters found with the SFSE and EMTSFM and corresponding relative errors ε

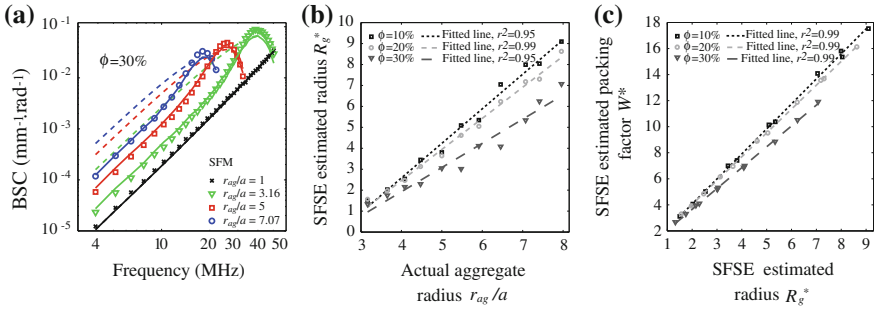

Fig. 6.10 **a** Frequency-dependent backscatter coefficients computed with the SFM for different aggregate sizes and a constant aggregate compactness $\phi_i = 60\ \%$ at a systemic hematocrit of 30 %, and corresponding fitting with the SFSE (in *dashed lines*) and with the EMTSFM (in *solid lines*). **b** Comparison of the estimated aggregate size R_g^* obtained with the SFSE to the true size r_{ag}/a for the three systemic hematocrits of 10, 20 and 30 %. **c** Linear relationship between W^* and R_g^*

estimated when the aggregate compactness varied (see Table 6.1), and the SFSE parameters W^* and R_g^* followed a linear relationship. It means that the BSC parameterization is reduced to one parameter physically linked to the aggregate size. On the other hand, the EMTSFM was the model that better matched the simulated data and gave quantitatively satisfactory estimates when the aggregate radius and compactness varied. At the moment, the SFSE is largely used because of a fast computation around 0.1 s to estimate parameters from a single BSC, against 1 s with the EMTSFM using Matlab programs (The MathWorks, Inc., Natick, MA). Also, the SFSE was developed to consider tissue attenuation for in vivo applications (Franceschini et al. 2008, 2010), whereas it is still not the case for the EMTSFM.

Table 6.2 Comparison of the SFSE and EMTSFM based on simulated BSCs for the following aggregating conditions: r_{ag}/a varies, $\phi = 30\,\%$, $\phi_i = 60\,\%$ (except in the case of diaggregated RBCs where $\phi_i = 100\,\%$)

SFM		SFSE			EMTSFM			
Actual r_{ag}/a	Actual ϕ_i (%)	Estimated W^*	Estimated R_g^*	$\varepsilon_{R_g^*}$ (%)	Estimated ϕ_i^* (%)	$\varepsilon_{\phi_i^*}$ (%)	Estimated r_{ag}^*/a	$\varepsilon_{r_{ag}^*}$ (%)
1	100	0.17	0.38	62.00	100	0.00	1.0	0.00
3.16	60	2.67	1.32	58.23	66	10.00	3.0	5.06
5	60	5.31	3.04	39.20	68	13.33	4.7	6.00
7.07	60	8.58	5.33	24.61	66	10.00	6.6	6.65

Values of the aggregate size r_{ag}/a and compactness ϕ_i used for computation of the simulated BSC_{SFM} from the SFM, and values of parameters found with the SFSE and EMTSFM and corresponding relative errors ε

6.5 In Vitro and In Vivo Experimental Studies

6.5.1 In Vitro Experiments

As seen previously in Sect. 6.3, computer simulations allowed to determine the influence of the aggregate size, shape and compactness on ultrasound backscattering. It is currently difficult to control all these parameters in in vitro experiments. An instructive in vitro experiment is to shear blood in a Couette flow device providing a linear velocity profile and a constant shear rate for a given rotational speed of the device (Foster et al. 1994; Van Der Heiden et al. 1995; Yu and Cloutier 2007; Yu et al. 2009). A homogeneous level of aggregation could thus be expected in such a controlled flow. Figure 6.11 shows the typical measured BSC_{meas} as a function of frequency for porcine blood at a systemic hematocrit of 40 % sheared at different shear rates in a Couette flow device (Franceschini et al. 2010). These experimental data were obtained using an ultrasound scanner Vevo 770, Visualsonics (Toronto, Canada) equipped with a 25 MHz-center frequency probe (RMV 710). The measured BSC_{meas} signifies here the experimental measure of the BSC. It was calculated here by a substitution method with a reference phantom (i.e. a sample of disaggregated RBCs suspended in saline at a 6 % hematocrit) to compensate the backscattered power spectra for the electromechanical system response, and the depth-dependent diffraction and focusing effects caused by the ultrasound beam. As observed in Fig. 6.11, the amplitude of the BSC_{meas} increases and the peak occurs at lower frequencies as the shear rate decreases (i.e. when the level of aggregation increases). Also represented are corresponding fitted curves obtained with the SFSE, as well as the corresponding values of W^*, D^* and the correlation coefficient r^2 to assess the goodness of fit between the model and the measured data. Note that in this section the aggregate sizes estimated by the SFSE correspond to the mean aggregate diameter D^* instead of the mean aggregate gyration radius R_g^* (see Eq. (6.13)). The SFSE provides good fits to the data and W^* and D^* increase when the shear rate decreases.

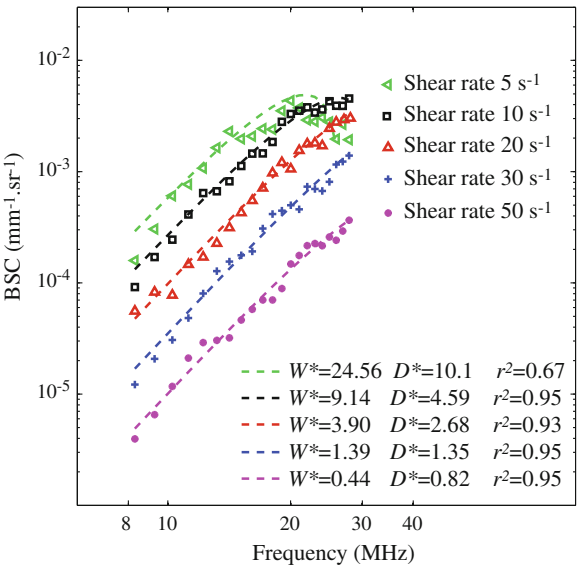

Fig. 6.11 Backscatter coefficients for blood sheared at different shear rates, and corresponding fitting with the SFSE (Figure modified from Franceschini et al. 2010)

The corresponding spatial maps of aggregate size and packing factor estimates (parametric images) for a shear rate of 10 s^{-1} are displayed in Fig. 6.12. The parametric images are superimposed on a conventional B-mode frame. The parametric images are useful for describing how aggregate structures vary in size as a function of depths. In the Couette flow experiments, the parametric images are quite homogenous as it was expected, since the level of aggregation is identical whatever the depth. Under in vivo conditions with ultrasound measurements on a blood vessel, the shear rate distribution varies with the radial position, and consequently, the aggregate size distribution too. An example of parametric images of porcine blood in a tubular in vitro experiment is displayed in Fig. 6.13.

6.5.2 In Vivo Experiments

The difficulty to apply the SFSE or the EMTSFM in vivo is that the spectral content of backscattered echoes is also affected by attenuation caused by intervening tissue layers (such as the skin) between the probe and the blood flow. To evaluate correctly microstructural parameters, it is thus of major interest to take into account tissue attenuation effects. Some groups (He and Greenleaf 1986; Oosterveld et al.1991) developed measurement techniques to evaluate the frequency-dependent attenuation in order to compensate *a posteriori* the backscattered power spectrum. Recently, Bigelow et al. (2005a, 2005b) introduced a new

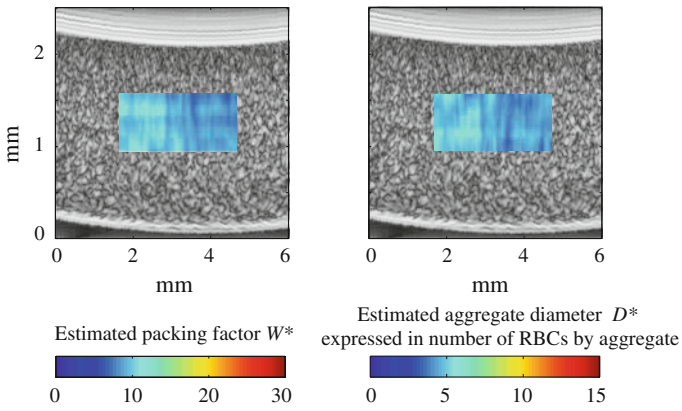

Fig. 6.12 Quantitative images of porcine blood sheared at 10 s^{-1} in a Couette device superimposed on the gray-scale B-mode images. Parameters W^* and D^* were estimated by the SFSE (Figure modified from Franceschini et al. 2010)

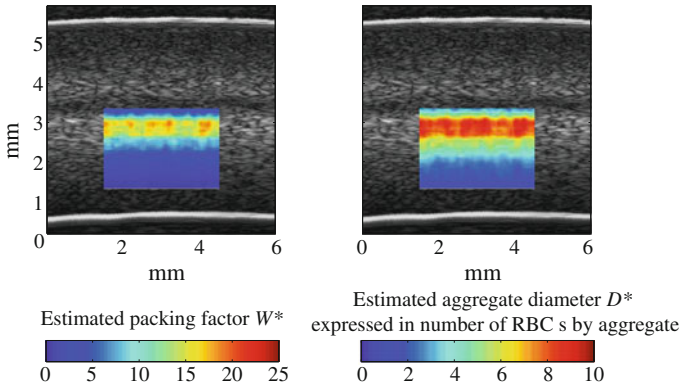

Fig. 6.13 Quantitative images of porcine blood sheared in a tube superimposed on the gray-scale B-mode images. Parameters W^* and D^* were estimated by the SFSE (Figure modified from Franceschini et al. 2010)

algorithm that has the advantage to estimate simultaneously the effective radius of the tissue microstructure and the total attenuation. These two parameters were determined by using a single minimization method that fits the spectrum of the backscattered RF echoes from the region of interest (ROI) to an estimated spectrum by an appropriate model. This last strategy was recently adapted for the estimation of RBC scatterer sizes by slightly modifying the SFSE and was named the Structure Factor Size and Attenuation Estimator (SFSAE) (Franceschini et al. 2008, 2010). The SFSAE allows to determine simultaneously blood structural parameters (i.e. W and D) and the total attenuation by modeling the theoretical backscattering coefficient of blood as follows (Franceschini et al. 2008):

$$\begin{aligned} BSC_{SFSAE}(-2k) &= n\sigma_b(-2k)\left(W - \frac{12}{5}(kaD)^2\right)A(-2k) \\ &\approx n\sigma_b(-2k)\left(W - \frac{12}{5}(kaD)^2\right)e^{\frac{-4\,\alpha_0\,kc}{8.68\,2\pi}} \end{aligned} \tag{6.17}$$

where A is the frequency-dependent attenuation function, c is the mean speed of sound in the intervening tissue layers and α_0 is the attenuation coefficient (in dB/MHz) defined by: $\alpha_0 = \sum_i \alpha_i e_i$, where α_i and e_i are respectively the intervening tissue layer attenuations (in dB/cm/MHz) and thicknesses. One can note in Eq. (6.17) the coefficient 8.68 that expresses unit conversion from dB to Neper: $\alpha_0[\text{Neper/MHz}] = \alpha_0[\text{dB/MHz}]/8.68$. According to the above equation, we thus assume that the attenuation increases linearly with the frequency f: $\alpha(f) = \alpha_0 f/8.68$. The packing factor W^*, aggregate diameter D^* and total attenuation along the propagation path α_0^* are determined by matching the measured BSC with the theoretical BSC_{SFSAE} given by Eq. (6.17), as performed previously with the SFSE model.

Note that the SFSAE allows to estimate a total attenuation, including the intervening tissues between the probe and the blood flow but also the blood attenuation itself. The skin is one of the most attenuating tissue layers during in vivo scanning. The attenuation of human dermis is around 0.21 dB/MHz at 14–50 MHz considering a 1-mm dermis thickness (Raju and Srinivasan 2001). On the other hand, the blood attenuation is smaller around 0.015 dB/mm/MHz for disaggregated blood and 0.053 dB/mm/MHz for large aggregating conditions (Franceschini et al. 2010).

With in vitro experiments (Franceschini et al. 2008, 2010) the method gave satisfactory estimates with relative errors below 25 % for attenuations between 0.115 and 0.411 dB/MHz and $D^* < 7.29$ (corresponding to a product $kr_{ag} < 2.08$). Measurements were also performed on an arm's vein of a normal subject using an ultrasound scanner equipped with a 25 MHz center frequency probe (Franceschini et al. 2009). The probe was positioned in longitudinal view to examine a complex flow in the vinicity of two closed venous valves. Regions were examined upstream and downstream from the two venous valves. Quantitative ultrasound parametric images of the aggregate diameter D^*, the packing factor W^* and the total attenuation α_0^* were constructed by using the SFSAE (Fig. 6.14). The black pixels in Fig. 6.14 correspond to rejected solutions of the optimization method, when the estimated packing factor W^* or diameter D^* was found equal to zero, which is unrealistic (see section V-D in Franceschini et al. 2010). For the two structural parameters D^* and W^*, statistically significant differences were observed between blood stagnation and circulation zones; whereas attenuation mean values were quite similar. This work shows the SFSAE ability to estimate blood structural properties in vivo and in situ, and opens the way to parametric imaging for clinical studies in abnormal blood conditions.

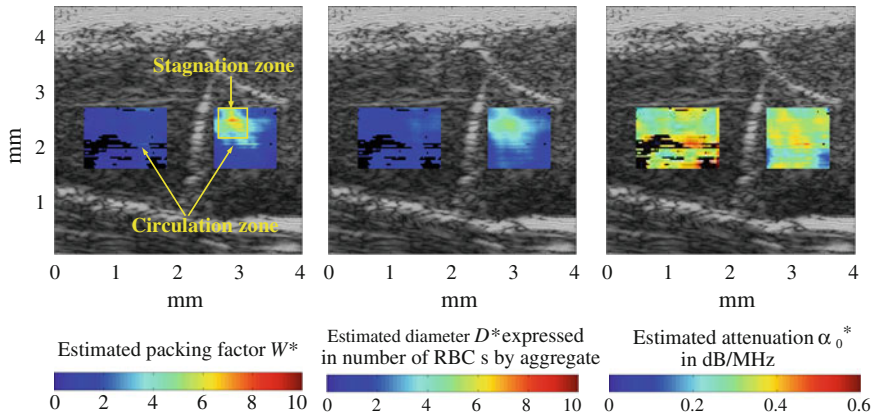

Fig. 6.14 Quantitative images of blood circulating in the vinicity of the two closed venous valves superimposed on the gray-scale B-mode images. Parameters W^*, D^* and α_0^* were estimated by the SFSAE (Figure modified from Franceschini et al. 2009)

6.6 Conclusion

This chapter has focused on the theoretical structure factor model of ultrasound backscattering by aggregated RBCs, on computer simulations to understand the impact of the aggregate structure on the frequency-dependent BSC and on two approximated theoretical models, the SFSE (or SFSAE) and the EMTSFM, allowing the estimation of blood structural properties. The SFSAE, i.e. the modified SFSE allowing to take into account the intervening tissue between the probe and the blood, has been shown able of estimating blood structural properties in vivo and in situ. Using the SFSAE, future works should focus on in vivo and in situ assessment of the pathophysiological impact of abnormal RBC aggregation on the cardiovascular system (see for example Yu et al. 2011).

The EMTSFM recently proposed is also a very promising model needing to be developed to speed the parameter estimation. Computed simulations show the superiority of the EMTSFM to estimate RBC aggregate size and compactness in comparison with the SFSE. An important contribution of this new model is the parameterization of the BSC with the aggregate compactness, which is a structural parameter not available in any other modeling strategies proposed in quantitative ultrasound imaging. The main limitation of the EMTSFM (as well as the SFSE) is the assumption of isotropic aggregates that limits the use of these models to pathological blood. In the future, improvements should consider incorporating the aggregate anisotropy and the possibility to simultaneously estimate the tissue attenuation, as for the SFSAE. It means that the EMTSFM could be slightly modified by introducing the attenuation term to estimate simultaneously the RBC aggregate size, compactness and the total attenuation.

Acknowledgments We acknowledge the continuous financial support of the Canadian Institutes of Health and Natural Sciences and Engineering Research Council of Canada, and the French National Center for Scientific Research (CNRS).

References

Anderson VC (1950) Sound scattering from a fluid sphere. J Acoust Soc Am 22:426–43

Angelsen BAJ (1980) Theoretical study of the scattering of ultrasound by blood. IEEE Trans Biomed Eng 27:61–67

Armstrong JK, Wenby RB, Meiselman HJ, Fisher TC (2004) The hydrodynamic radii of macromolecules and their effect on red blood cell aggregation. Biophys J 87:4259–4270

Berger NE, Lucas RJ, Twersky V (1991) Polydisperse scattering theory and comparisons with data for red blood cells. J Acoust Soc Am 89:1394–1401

Bigelow TA, Oelze ML, O'Brien WD (2005a) Estimation of total attenuation and scatterer size from backscatter ultrasound waveforms. J Acoust Soc Am 117:1431–1439

Bigelow TA, O'Brien WD (2005b) Signal processing strategies that improve performance and understanding of the quantitative ultrasound SPECTRAL FIT algorithm. J Acoust Soc Am 118:1808–1819

Chabanel A, Horellou MH, Conard J, Samama MM (1994) Red blood cell aggregability in patients with a history of leg vein thrombosis: influence of post-thrombotic treatment. Br J Haematol 88:174–179

Chien S (1975) Biophysical behavior of red cells in suspensions. In: Surgenor DM (ed) The red blood cell. Academic, New York

Cloutier G, Qin Z (1997) Ultrasound backscattering from non-aggregating and aggregating erythrocytes—a review. Biorheology 34:443–470

Cloutier G, Daronat M, Savery D, Garcia D, Durand LG, Foster FS (2004) Non-Gaussian statistics and temporal variations of the ultrasound signal backscattered by blood at frequencies between 10 and 58 MHz. J Acoust Soc Am 116:566577

Cloutier G, Zimmer A, Yu FT, Chiasson JL (2008) Increased shear rate resistance and fastest kinetics of erythrocyte aggregation in diabetes measured with ultrasound. Diabet Care 31:1400–1402

Coussios CC (2002) The significance of shape and orientation in single-particle weak-scatterer models. J Acoust Soc Am 112:906-915

De Kroon MGM, Slager CJ, Gussenhoven WJ, Serruys PW, Roelandt JRTC, Bom N (1991) Cyclic changes of blood echogenicity in high frequency ultrasound. Ultrasound Med Biol 17:723–728

Le Dévéhat C, Khodabandehlou T, Vimeux M, Aouane F (1996) Diabetes mellitus: its effects on blood rheological properties and microcirculatory consequences. Clin Hemorheol 16:677–683

Feleppa EJ, Lizzi FL, Coleman DJ, Yaremko MM (1986) Diagnostic spectrum analysis in ophthalmology: a physical perspective. Ultrasound Med Biol 12:623–631

Feleppa EJ, Liu T, Kalisz A, Shao MC, Fleshner N, Reuter V (1997) Ultrasonic spectral-parameter imaging of the prostate. Int J Imag Syst Technol 8:11–25

Fontaine I, Bertrand M, Cloutier G (1999) A system-based approach to modeling the ultrasound signal backscattered by red blood cells. Biophys J 77:2387–2399

Fontaine I, Savery D, Cloutier G (2002) Simulation of ultrasound backscattering by red blood cell aggregates: effect of shear rate and anisotropy. Biophys J 82:1696–1710

Fontaine I, Cloutier G (2003) Modeling the frequency dependence (5–120 MHz) of ultrasound backscattering by red cell aggregates in shear flow at a normal hematocrit. J Acoust Soc Amer 113:2893–2900

Foster FS, Obara H, Bloomfield T, Ryan LK, Lockwood GR (1994) Ultrasound backscatter from blood in the 30–70 MHz frequency range. In: Proceedings IEEE Ultrasonic Symposium, pp 1599–1602

Franceschini E, Yu FTH, Destrempes F, Cloutier G (2010) Ultrasound characterization of red blood cell aggregation with intervening attenuating tissue-mimicking phantoms. J Acoust Soc Amer 127:1104–1115

Franceschini E, Yu FTH, and Cloutier G (2008) Simultaneous estimation of attenuation and structure parameters of aggregated red blood cells from backscatter measurements. J Acoust Soc Am 123:EL85-91

Franceschini E, Yu FTH, Destrempes F, Cloutier G (2009) In vivo ultrasound characterization of red blood cell aggregation using the structure factor size and attenuation estimator. In: Proceedings IEEE ultrasonic symposium, pp 301–304

Franceschini E, Metzger B, and Cloutier G (2011) Forward problem study of an effective medium model for ultrasound blood characterization. IEEE Trans Ultras Ferroelectr Freq Control 58:2668–2679

Guinier A, Fournet J (1955) Small angle scattering of X-rays. Wiley Interscience, New York

Hayakawa M, Kuzuya F (1991) Effects of ticlopidine on erythrocytes aggregation in thrombotic disorders. Angiology 42:747–753

He P, Greenleaf JF (1986) Application of stochastic analysis to ultrasonic echoes—estimation of attenuation and tissue heterogeneity from peaks of echo envelope. J Acoust Soc Am 79:526–534

Hunt JW, Worthington AE, Kerr AT (1995) The subtleties of ultrasound images of an ensemble of cells: simulation from regular and more random distributions of scatterers. Ultrasound Med Biol 21:329–341

Insana MF, Wagner RF, Brown DG, Hall TJ (1990) Describing small-scale structure in random media using pulse-echo ultrasound. J Acoust Soc Am 87:179–192

Insana MF, Brown DG (1993) Acoustic scattering theory applied to soft biological tissues. In: Shung KK, Thieme GA (eds) Ultrasonic scattering in biological tissues. CRC, Boca Raton, FL

Kolios MC, Czarnota GJ, Lee M, Hunt JW, Sherar MD (2002) Ultrasonic spectral parameter characterization of apoptosis. Ultrasound in Med Biol 28:589–597

Kuster GT, Toksoz MN (1974) Velocity and attenuation of seismic waves in two-phase media: part I theoretical formulations. Geophysics 39:587–606

Lim B, Cobbold RSC (1999) On the relation between aggregation, packing and the backscattered ultrasound signal for whole blood. Ultrasound Med Biol 25:1395–1405

Lizzi FL, Ostromogilsky M, Feleppa EJ, Rorke MC, Yaremko MM (1986) Relationship of ultrasonic spectral parameters to features of tissue microstructure. IEEE Trans Ultrason Ferroelect Freq Contr 33:319–329

Lizzi FL, Astor M, Kalisz A, Liu T, Coleman DJ, Silverman R, Ursea R, Rondeau M (1996) Ultrasound spectrum analysis for different scatter morphologies: theory and very-high frequency clinical results. In: Proceedings IEEE Ultrason Symp, pp 1155–1159

Lucas RJ, Twersky V (1987) Inversion of ultrasonic scattering data for red blood cell suspensions under different flow conditions. J Acoust Soc Am 82:794–799

Madsen EL, Insana MF, Zagzebski JA (1984) Method of data reduction for accurate determination of acoustic backscatter coefficients. J Acoust Soc Am 76:913–923

Mamou J, Coron A, Hata M, Machi J, Yanagihara E, Laugier P, Feleppa E (2010) Three-dimensional high-frequency characterization of cancerous lymph nodes. Ultrasound Med Biol 36:361–375

Meiselman HJ (1993) Red blood cell role in RBC aggregation: 1963–1993 and beyond. Clin Hemorheol 13:575–592

Mo LYL and Cobbold RSC (1986) A stochastic model of the backscattered Doppler ultrasound from blood. IEEE Trans Biomed Eng 33:20–27

Mo LYL and Cobbold RSC (1992) A unified appraoch to modeling the backscattered Doppler ultrasound from blood. IEEE Trans Biomed Eng 39:450–461

Mo LYL, Cobbold RSC (1993) In: Shung KK, Thieme GA (eds) Ultrasonic scattering in biological tissues. CRC, Boca Raton, FL

Neumann FJ, Katus HA, Hoberg E, Roebruck P, Braun M, Haupt HM, Yillmanns H, Kubler W (1991) Increased plasma viscosity and erythrocyte aggregation: Indicators of an unfavorable clinical outcome in patients with unstable angina pectoris. Br Heart J 66:425–430

Nguyen LC, Yu FT, Cloutier G (2008) Cyclic changes in blood echogenicity under pulsatile flow are frequency dependent. Ultrasound Med Biol 34:664–673

Oelze ML, Zachary JF (2006) Examination of cancer in mouse models using high frequency quantitative ultrasound. Ultrasound Med Biol 32:1639–1648

Oosterveld BJ, Thijssen JM, Hartman PC, Romijn RL and Rosenbusch GJE (1991) Ultrasound attenuation and texture analysis of diffuse liver disease: methods and preliminary results. Phys Med Biol 36:1039–1064

Poggi M, Palareti G, Biagi R, Parenti M, Babini AC, Coccher S (1994) Prolonged very low calory diet in highly obese subjects reduces plasma viscosity and red cell aggregation but not fibrinogen. Int J Obes 18:490–496

Raju I, Srinivasan MA (2001) High-frequency ultrasonic attenuation and backscatter coefficients of in vivo normal human dermis and subcutaneous fat. Ultrasound Med Biol 27:15431556

Rampling MW, Meiselman HJ, Neu B, Baskurt OK (2004) Influence of cell-specific factors on red blood cell aggregation. Biorheology 41:91–112

Routh HF, Gough W, Williams RP (1987) One-dimensional computer simulation of a wave incident on randomly distributed inhomogeneities with reference to the scattering of ultrasound by blood. Med Biol Eng Comput 25:667–671

Saha RK, Cloutier G (2008) Monte Carlo study on ultrasound backscattering by three-dimensional distributions of red blood cells. Physical Review E 78:061919

Saha RK, Franceschini E, Cloutier G (2011) Assessment of accuracy of the structure-factor-size-estimator method in determining red blood cell aggregate size from ultrasound spectrum backscattering coefficient. J Acoust Soc Am 129:2269–2277

Savery D, Cloutier G (2001) A point process approach to assess the frequency dependence of ultrasound backscattering by aggregating red blood cells. J Acoust Soc Am 110:3252–3262

Savery D, Cloutier G (2005) Effect of red cell clustering and anisotropy on ultrasound blood backscatter: a Monte Carlo study. IEEE Trans Ultras Ferroelectr Freq Control 52:94–103

Savery D, Cloutier G (2007) High-frequency ultrasound backscattering by blood: analytical and semi-analytical models of the erythrocyte cross section. J Acoust Soc Amer 23:3963–3971

Schmid-Schönbein H, Gallasch G, Gosen JV, Volger E, Klose HJ (1976) Red cell aggregation in blood flow. I New methods of quantification. Klin Wschr 54:149–157

Schmid-Schönbein H, Malotta H, Striesow F (1990) Erythrocyte aggregation: causes, consequences and methods of assessment. Tijdschr NVKS 15:88–97

Shung KK (1982) On the ultrasound scattering from blood as a function of hematocrit. IEEE Trans Sonics Ultrason SU-29:327–331

Stoltz JF, Donner M (1991) Red blood cell aggregation: measurements and clinical applications. Tr J Med Sci 15:26–39

Teh BG, Cloutier G (2000) Modeling and analysis of ultrasound backscattering by spherical aggregates and rouleaux of red blood cells. IEEE Trans Ultras Ferroelectr Freq Control 47:1025–1035

Twersky V (1987) Low-frequency scattering by correlated distributions of randomly oriented particles. J Acoust Soc Am 81:1609–1618

Van Der Heiden MS, De Kroon MGM, Bom N, Borst C (1995) Ultrasound backscatter at 30 MHz from human blood: influence of rouleau size affected by blood modification and shear rate. Ultrasound Med Biol 21:817–826

Vayá A, Falcó C, Rganon E, Vila V, Martnez-Sales V, Corella D, Contreras MT, Aznar J (2004) Influence of plasma and erythrocyte factors on red blood cell aggregation in survivors of acute myocardial infarction. Thromb Haemost 91:354–359

Wang SH, Shung KK (1997) An approach for measuring ultrasonic backscattering from biological tissues with focused transducers. IEEE Trans Biomed Eng 44:549–554

Weng X, Cloutier G, Pibarot P, Durand LG (1996a) Comparison and simulation of different levels of erythrocyte aggregation with pig, horse, sheep, calf, and normal human blood. Biorheology 33:365–377

Weng X, Cloutier G, Beaulieu R, Roederer GO (1996b) Influence of acute-phase proteins on erythrocyte aggregation. Am J Physiol 271:H2346–H2352 (Heart and Circulatory, Physiology 40)

Yu FTH, Cloutier G (2007) Experimental ultrasound characterization of red blood cell aggregation using the structure factor size estimator. J Acoust Soc Am 122:645–656

Yu FTH, Franceschini E, Chayer B, Armstrong JK, Meiselman HJ, Cloutier G (2009) Ultrasonic parametric imaging of erythrocyte aggregation using the structure factor size estimator. Biorheology 46:343363

Yu FTH, Armstrong JK, Tripette J, Meiselman HJ, Cloutier G (2011) A local increase in red blood cell aggregation can trigger deep vein thrombosis: evidence based on quantitative cellular ultrasound imaging. J Thrombosis Haemostasis 9:481–488

Yuan YW, Shung KK (1988) Ultrasonic backscatter from flowing whole blood. I: dependence on shear rate and hematocrit. J Acoust Soc Am 84:52–58

Zhang J, Rose JL, Shung KK (1994) A computer model for simulating ultrasonic scattering in biological tissues with high scatterer concentration. Ultrasound Med Biol 20:903–913

Zijlstra WG, Mook GA (1962) Medical reflection photometry. In: Van Gorcum (ed) Assen, Netherlands